AGU PUBLICATIONS

JGR

Journal of Geophysical Research: Solid Earth

RESEARCH ARTICLE
10.1002/2015JB012084

Special Section:
Stress, Strain and Mass Changes at Volcanoes

Moment tensors associated with the expansion and movement of fluid in ellipsoidal cavities

Naoto Mizuno[1], Mie Ichihara[2], and Nobuki Kame[2]

[1]Department of Earth and Planetary Science, Graduate School of Science, The University of Tokyo, Tokyo, Japan, [2]Earthquake Research Institute, The University of Tokyo, Tokyo, Japan

Key Points:
- Diagram to assess moment tensor component ratio is extended for two ellipsoids
- Our method is useful in inferring the source processes from moment tensors
- Fluid mechanical constraints are included to relate moment tensors and processes

Correspondence to:
N. Mizuno,
mizuno@eps.s.u-tokyo.ac.jp

Citation:
Mizuno, N., M. Ichihara, and N. Kame (2015), Moment tensors associated with the expansion and movement of fluid in ellipsoidal cavities, *J. Geophys. Res. Solid Earth*, *120*, doi:10.1002/2015JB012084.

Received 1 APR 2015
Accepted 9 JUL 2015
Accepted article online 14 JUL 2015

Abstract Moment tensor representation is useful for interpreting source processes from seismic and/or geodetic observations. However, there remains difficulty to determine the source processes because some models cannot be distinguished from moment tensors and the range of moment tensor represented by particular process is generally limited. We examine magma movement between two ellipsoids with consideration of mass conservation and pressure balance. The resultant moment tensor component ratio (MTCR) range is clearly distinguished from that generated by expanding ellipsoids. However, there is a range of the MTCR that cannot be explained by either fluid expansion or movement; in such cases, partial pressure recovery after fluid movement provides a plausible explanation. The MTCR for fluid movement between two ellipsoids with randomly varying geometry and relative orientation is shown to exhibit a concentrated trend representing a linear combination of a double-couple source and an opening crack. Although such an MTCR is generally interpreted as a crack with both tensile and shear dislocations, we demonstrate that it can be generated by fluid movement between two thin ellipsoids. Our results provide a physically reasonable mechanism for interpreting the MTCR obtained from observed data with a comprehensive view of possible source processes.

1. Introduction

Moment tensor inversion is widely used in seismological and volcanological research to infer source processes from seismic and/or geodetic signals. A typical earthquake source mechanism is a shear dislocation across a fault that does not include volumetric change. However, moment tensor inversions in active volcanic regions frequently include volumetric components. Such observations indicate pressure change inside a volcano due to fluid movement (magma and/or gas) or a phase transition (magma degassing). The identification and quantification of these processes are important in understanding and forecasting volcanic activity.

A seismic or geodetic moment tensor is generally represented by a symmetric 3×3 matrix that can be diagonalized by a rotation of axes. The three diagonal components represent the eigenvalues of the moment tensor, giving information regarding the mechanism, geometry, and volume change of the source.

Problems often arise in interpreting particular source processes from moment tensors. The volume changes represented by the moment tensor and the actual volume change are different, and their relation is nonunique. The classical theory that links the source volume change to the moment tensor components has been explained by *Aki and Richards* [1980], based on the stress-free transformation [*Eshelby*, 1957]. However, the physical meaning of the stress-free transformation has not been clearly explained. In addition, its quantitative relationship to the actual volume change has only been shown for specific source models with simple geometries (e.g., a sphere, a cylinder, a crack, or an ellipsoid), and its general relationship to arbitrary geometries remains unknown. In fact, there are discrepancies regarding the volume change to be used in the moment tensor [*Wielandt*, 2003; *Richards and Kim*, 2005; *Kumagai et al.*, 2014]. *Kumagai et al.* [2014] explicitly showed that isotropic source models, such as an expanding sphere and a set of three perpendicular open cracks, all of which generate an identical isotropic moment tensor, result in different volume changes.

It should be noted that the moment tensor representation is based solely on the elastodynamic framework. While it considers elastic deformation outside the source, it does not consider fluid mechanical constraints for the material inside the source, which include mass conservation, pressure balance, and the compressibility of the fluid in the source. Although the obtained moment tensors are often interpreted by a linear combination of elementary point sources, such as the expansion of a sphere, a cylinder, a crack, or an ellipsoid, and

CLVD (compensated linear vector dipole), which is thought to represent fluid movement [e.g., *Chouet*, 1996; *Kumagai*, 2009], these interpretations do not necessarily take into account fluid mechanical constraints.

Recent studies have tried to bridge the gap between seismological source representation using a moment tensor and fluid mechanical modeling of volcanic processes. *Kumagai et al.* [2014] demonstrated how the relation between the moment tensor and source volume change depends on the source medium, specifically for a spherical source. The volume change obtained from the VLP (very long period) pulse has been compared with SO_2 emissions at Asama volcano, Japan [*Kazahaya et al.*, 2011, 2015]. The above mentioned problems in connecting the moment tensor to the source fluid mechanics were encountered when trying to interpret the VLP moment tensors as the mass movement of gas, which were considered to be causes of the VLP events. The simplest assumption for a source representation of fluid movement is that the volume gained by the downstream cavity equals the volume lost by the upstream one so that the net volume change is zero. A CLVD source is one such example. *Amoruso and Crescentini* [2013] considered the simultaneous expansion and contraction of two cavities where the total actual volume change is zero. They showed that the apparent volume change obtained from the total moment tensor is not zero and that its sign can be positive or negative. In fact, such an assumption of zero total volume change is invalid when one takes into account the effects of fluid compressibility and phase transition [*Rivalta*, 2010; *Rivalta and Segall*, 2008; *Nishimura*, 2004]. It is important to note that volume conservation and mass conservation are not equivalent, with the latter being an essential constraint in fluid mechanics.

Here we discuss fluid mechanical constraints on ellipsoidal sources. First, we summarize the relation between volume changes and the moment tensor representation of an ellipsoidal source, following *Davis* [1986] and *Amoruso and Crescentini* [2009]. A convenient diagram of the moment tensor component ratio (MTCR) proposed for a single ellipsoid [*Trasatti et al.*, 2009, 2011; *Amoruso and Crescentini*, 2013] is employed and extended for two-ellipsoidal expanding cavities with pressure balance. We then examine magma movement processes where mass conservation and pressure balance are considered. We also examine the effect of partial pressure recovery after magma movement, which is likely to occur in natural systems [*Nishimura*, 2004]. Through these investigations, we clarify the possibilities and limitations of source constraints obtained from observed moment tensors.

2. A Brief Summary of Moment Tensor Representation of a Volume Source

This section is based mainly on classical studies [*Eshelby*, 1957; *Aki and Richards*, 1980; *Davis*, 1986], setting the framework for the moment tensor study presented here. The theoretical results of these studies are summarized with the notation conventionally used: superscript *C* and *T* represent the actual deformation and the stress-free deformation, respectively.

A cavity embedded in an elastic medium has been considered as the volume source with a reference volume V prior to volumetric deformation [*Aki and Richards*, 1980, 2002]. Here the cavity is assumed to be filled with fluid, following *Davis* [1986]. When the cavity undergoes volumetric deformation due to fluid pressure change ΔP, deformation of the cavity is characterized by two distinct strains: stress-free strain e_{ij}^T and the actual strain e_{ij}^C [*Eshelby*, 1957]. The moment tensor of the volume source is represented by the stress-free strain as

$$M_{ij} = c_{ijkl} e_{kl}^T V, \tag{1}$$

where c_{ijlk} is the elastic constant tensor [*Aki and Richards*, 1980].

For this moment tensor representation and source modeling, e_{ij}^T and e_{ij}^C must be determined. These strains are related by

$$e_{ij}^C = S_{ijkl} e_{kl}^T, \tag{2}$$

where S_{ijkl} is a linear operator depending on the cavity geometry and c_{ijkl}. Another relationship is given by the stress boundary condition at the inner cavity wall as

$$c_{ijkl}\left(e_{kl}^T - e_{kl}^C\right) = \Delta P \delta_{ij}, \tag{3}$$

where $\Delta P \delta_{ij}$ is the isotropic stress component due to fluid overpressure. We consider a symmetric case in solving the coupled equations (equations (2) and (3)), where both e_{ij}^T and e_{ij}^C have only diagonal components.

This is valid for a symmetric cavity geometry, such as a sphere, a cylinder, a penny-shaped crack, or an ellipsoid, because of the invariance of the strain tensor components under the rotation of 180°. For these symmetric geometries, the exact form of S_{ijkl} has been derived. The diagonal components and relevant elastic constants are denoted by

$$\epsilon_i = e_{ij}|_{i=j}, \tag{4}$$

$$S'_{ik} = S_{ijkl}|_{i=j,k=l}, \tag{5}$$

$$c'_{ik} = c_{ijkl}|_{i=j,k=l}. \tag{6}$$

Equations (2) and (3) can then be rewritten as

$$\epsilon_i^C = S'_{ij}\epsilon_j^T, \tag{7}$$

$$c'_{ij}(\epsilon_j^T - \epsilon_j^C) = \Delta P U_i, \tag{8}$$

where U_i represents a vector with all components being one. Equations (7) and (8) are then combined to give

$$c'_{ij}\left(\delta_{jk} - S'_{jk}\right)\epsilon_k^T = \Delta P U_i. \tag{9}$$

With the following relationships

$$K_{ji} = c'^{-1}_{ij}, \tag{10}$$

$$D_{ji} = (\delta_{ij} - S'_{ij})^{-1}, \tag{11}$$

we finally obtain

$$\epsilon_i^T = \Delta P D_{ij} K_{jk} U_k, \tag{12}$$

$$\epsilon_i^C = \Delta P S'_{ij} D_{jk} K_{kl} U_l. \tag{13}$$

The volume change of the cavity is given by the product of the trace of the strain tensor and the reference volume V. The stress-free volume change ΔV^T and the actual volume change ΔV^C are

$$\Delta V^T = V U_i \epsilon_i^T = V \Delta P U_i D_{ij} K_{jk} U_k, \tag{14}$$

$$\Delta V^C = V U_i \epsilon_i^C = V \Delta P U_i S'_{ij} D_{jk} K_{kl} U_l, \tag{15}$$

respectively. Finally, the moment tensor for the fluid cavity source is represented in terms of the stress-free volume change as follows:

$$M_{ij}|_{i=j} = c'_{ik} \frac{D_{kl} K_{lm} U_m}{U_p D_{pq} K_{qr} U_r} \Delta V^T. \tag{16}$$

In the above equations c_{ijkl} is not limited to the isotropic medium. We hereafter consider an isotropic elastic medium, where

$$c_{ijkl} = \lambda \delta_{ij}\delta_{kl} + \mu(\delta_{ik}\delta_{jl} + \delta_{il}\delta_{jk}), \tag{17}$$

and λ and μ are the Lamé constants. The bulk modulus k and Poisson's ratio ν of the medium are represented as

$$k = \lambda + \frac{2}{3}\mu, \tag{18}$$

$$\nu = \frac{\lambda}{2(\lambda+\mu)}, \tag{19}$$

respectively. $K_{ij}U_j = c_{ji}^{-1}U_j$ is then reduced to

$$K_{ij}U_j = \frac{U_i}{3\lambda+2\mu} = \frac{U_i}{3k}. \tag{20}$$

With the use of the bulk modulus, equations (12)–(15) are rewritten as

$$\epsilon_i^T = \frac{\Delta P}{3k}D_{ij}U_j, \tag{21}$$

$$\epsilon_i^C = \frac{\Delta P}{3k}S'_{ij}D_{jk}U_k, \tag{22}$$

$$\Delta V^T = \frac{V\Delta P}{3k}U_iD_{ij}U_j, \tag{23}$$

$$\Delta V^C = \frac{V\Delta P}{3k}U_iS'_{ij}D_{jk}U_k. \tag{24}$$

To examine the geometric effect of this cavity source, we define two specific quantities: Ψ and K^C. Ψ is the ratio of the actual volume change to the stress-free volume change:

$$\Psi = \frac{\Delta V^C}{\Delta V^T} = \frac{U_iS'_{ij}D_{jk}U_k}{U_lD_{lm}U_m}, \tag{25}$$

and K^C is the effective bulk modulus of the cavity, which is the ratio of the actual pressure change to the pressure change corresponding to the volumetric strain:

$$K^C = \frac{\Delta P}{k\frac{\Delta V^C}{V}} = \frac{3}{U_iS'_{ij}D_{jk}U_k}. \tag{26}$$

Defining these parameters makes the following expressions simpler, and similar parameters have been used in the previous studies. *Amoruso and Crescentini* [2013] used R_{iso} as the corresponding parameter for Ψ, while *Amoruso and Crescentini* [2009] used R_V for $(K^C)^{-1}$, both of which are normalized by the values for a sphere.

With reference to equations (25) and (26), equation (23) is reduced to

$$\Delta V^T = \frac{V\Delta P}{k\Psi K^C}, \tag{27}$$

and equation (16) to

$$M_{ij}|_{i=j} = \left(\lambda U_i + 2\mu\frac{\delta_{ik}D_{kl}U_l}{U_mD_{mn}U_n}\right)\Delta V^T. \tag{28}$$

The trace of equation (28) has a simple form:

$$M_{ii} = (3\lambda+2\mu)\Delta V^T = 3k\Delta V^T, \tag{29}$$

where the trace is proportional to ΔV^T with a fixed coefficient $3k$, irrespective of the source geometry. Accordingly, Ψ in equation (25) is proportional to $\Delta V^C/M_{ii}$.

Each of the diagonal components M_{ij} in equation (28) varies with the source geometry. For typical simple sources, the components can be easily evaluated by using the geometric symmetry:

1. Sphere
   The isotropic geometry leads to $D_{1j}U_j = D_{2j}U_j = D_{3j}U_j = \frac{1}{3}U_iD_{ij}U_j$. The diagonal components of the moment tensor are written as

$$M_{11} = M_{22} = M_{33} = \left(\lambda + \frac{2}{3}\mu\right)\Delta V^T. \tag{30}$$

   Equation (30) corresponds to equation (3.35) in *Aki and Richards* [2002].
2. Cylinder
   Consider a cylinder with its axis along the x_3 direction. In the case of axis-symmetric plane strain, the stress-free strain components are $\epsilon_1 = \epsilon_2$ and $\epsilon_3 = 0$. Equation (21) gives the stress-free strain as $D_{1j}U_j = D_{2j}U_j = \frac{1}{2}U_iD_{ij}U_j$ and $D_{3j}U_j = 0$. The diagonal components are written as

$$M_{11} = M_{22} = (\lambda + \mu)\Delta V^T, \quad M_{33} = \lambda\Delta V^T. \tag{31}$$

3. Penny-shaped crack
   Consider a penny-shaped crack on the $x_2 - x_3$ plane, having nonzero strain only in the x_1 direction. Equation (21) gives the stress-free strain as $D_{1j}U_j = U_iD_{ij}U_j$, $D_{2j}U_j = D_{3j}U_j = 0$. The diagonal components are written as

$$M_{11} = (\lambda + 2\mu)\Delta V^T, \quad M_{22} = M_{33} = \lambda\Delta V^T. \tag{32}$$

2.1. Ellipsoidal Volume Sources

To evaluate the moment tensor components for an elliptical source, we must calculate D_{ij}. The calculation procedure is briefly given in Appendix A. We summarize the characteristics of an ellipsoidal volume source, which have been presented previously [*Davis*, 1986; *Amoruso and Crescentini*, 2009, 2013; *Trasatti et al.*, 2009, 2011].

Figure 1 shows how Ψ and K^C change with geometry. The curve of the effective bulk modulus K^C is comparable to Figure 2 of *Amoruso and Crescentini* [2009] for R_V ($R_V \propto (K^C)^{-1}$). K^C becomes smaller as the geometry approaches a penny shape, suggesting that the pressure change for a fixed volume change can vary by many orders of magnitude, depending on the geometry. On the other hand, Ψ varies with the geometry by a simple factor: the maximum being 1 for a crack and the minimum being $\left(\lambda + \frac{2}{3}\mu\right)/(\lambda + 2\mu)$ for a sphere [*Aki and Richards*, 2002].

Figure 2 shows how the moment tensor diagonal components (eigenvalues) change with geometry as a function of the two moment tensor component ratios (MTCR) [*Trasatti et al.*, 2009, 2011; *Amoruso and Crescentini*, 2013]. The maximum, medium, and minimum diagonal components are indicated by M_{11}, M_{22}, and M_{33}, respectively. S, B, and P indicate the MTCR values for a sphere, a prolate ellipsoid, and a penny-shaped crack, respectively. For the area bounded by SBX, the directions of M_{11}, M_{22}, and M_{33} are in the directions of the shortest, medium, and longest axes of the ellipsoid, respectively, where $a_1 \le a_2 \le a_3$. However, in the range where M_{22}/M_{11} is smaller than X, M_{22} and M_{33} are in the directions of the longest and medium axes, respectively, and $a_1 \le a_3 \le a_2$. The MTCR is insensitive to geometry near X, which also results in large uncertainties in estimates of the effective bulk modulus and the corresponding pressure change.

We add the following remarks in addition to the above mentioned summary of the previous studies:

1. B is associated with a prolate ellipsoid, $a_1 = a_2 \ll a_3$, where the moment tensor approaches

$$M_{11} = M_{22} = \left(\lambda + \frac{7}{8}\mu\right)\Delta V^T, \quad M_{33} = \left(\lambda + \frac{1}{4}\mu\right)\Delta V^T. \tag{33}$$

   The expression is different from the conventional expression for a cylindrical source in equation (31), which is shown in Figure 2 by C. The cylindrical source model does not consider the strain component along the cylinder axis, which is unrealistic.
2. By varying the relative angles of their axes and the relative sizes of the cavities, a linear combination of two ellipsoidal expanding sources can generate the MTCR in the area bounded by SCP in Figure 2. For example, C is generated by two perpendicular cracks that expand equally. S is generated by $(M_{11}, M_{22}, M_{33}) = (1, 1, 3)$, representative of a crack and $(6, 6, 4)$, representative of a prolate spheroid. Many other combinations of

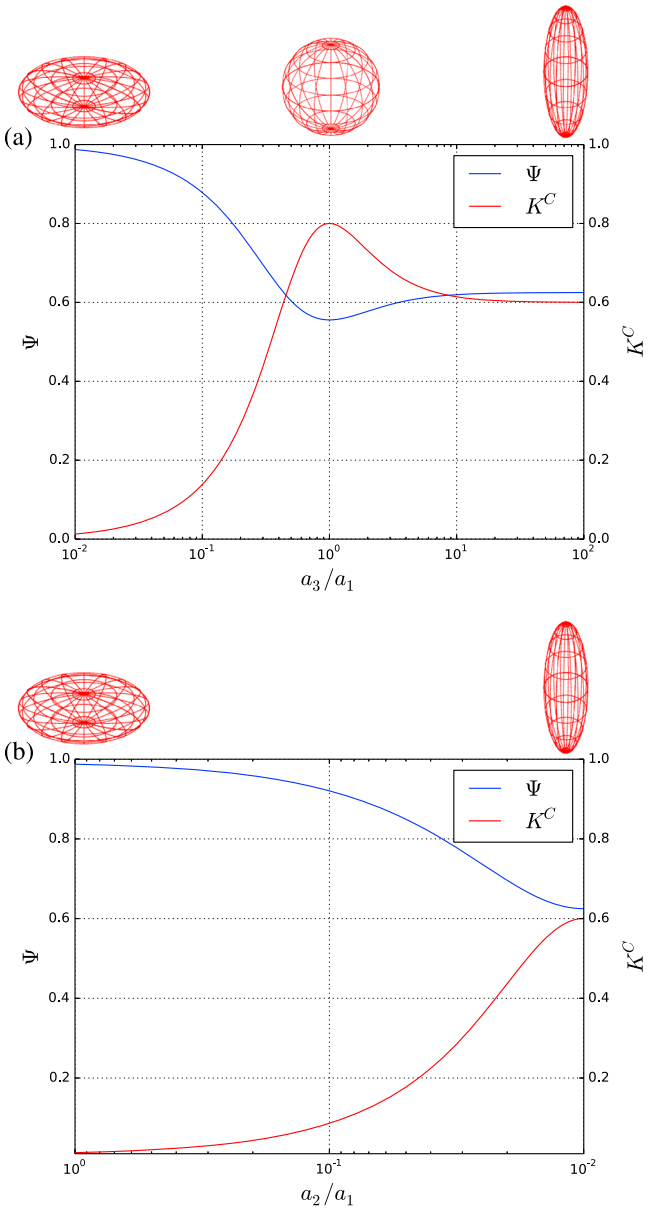

Figure 1. Geometrical dependencies of the volume ratio Ψ and the effective bulk modulus K^C: (a) as a function of a_3 where $a_1 = a_2$, where the geometry changes from a penny-shaped crack to a sphere and a cylinder, and (b) as a function of a_2 where $a_1 \gg a_3$, where the geometry changes from a penny-shaped crack to a cylinder. All of Figures 1–3 are plotted under the assumptions that $\lambda = \mu$ and Poisson's ratio $\nu = 1/4$.

two or more ellipsoids are also possible. This is in contrast to the result that an expanding source of a single ellipsoid can generate the MTCR only in the area SXPXBS. The range of the MTCR related to the 1970 deformation at Kilauea volcano, Hawaii, (solid triangle in Figure 2) lies outside of the permitted range of the MTCR generated by a single expanding ellipsoid [*Amoruso and Crescentini*, 2009]. However, it is in the area SCP, suggesting that a combination of two expanding ellipsoids can explain the moment tensor.

3. Volume Source Due To Fluid Movement Between Two Ellipsoidal Cavities

We have shown the possible range of the MTCR associated with ellipsoidal volume sources in section 2; the range is limited, and observed moment tensors do not always fall within the range. For example, the observed moment tensors for Asama volcano [*Maeda*, 2009; *Maeda and Takeo*, 2011] are shown by triangles in Figure 2, some of which are out of the range of SCP.

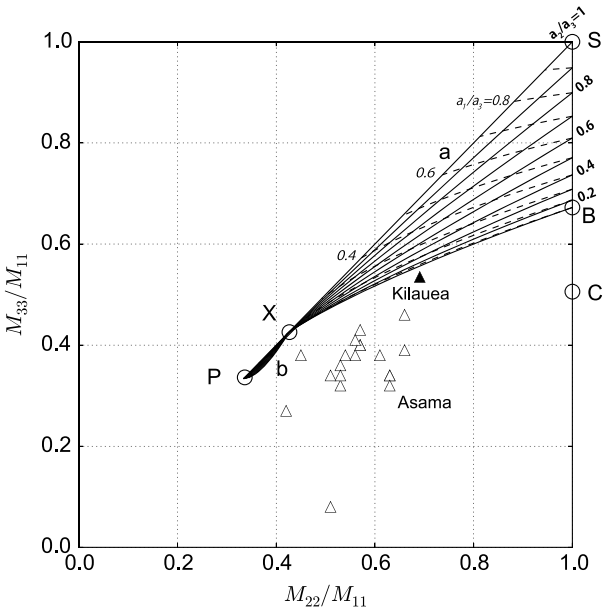

Figure 2. The possible range of the MTCR for an ellipsoidal volume source. The ratio a_1/a_3 is varied as indicated by bold labels along the solid contour lines for a constant a_2/a_3, while a_2/a_3 is varied as indicated by italic labels along the dashed contour lines for a constant a_1/a_3. S, B, and P indicate the MTCR values for a sphere, a prolate ellipsoid, and a penny-shaped crack, respectively, and C corresponds to the conventional cylinder model. The contour lines collapse at X, which marks where $a_2 = a_3$. The observed moment tensor for the 1970 deformation at Kilauea, Hawaii [*Davis*, 1986], and that for VLP observed at Asama, Japan [*Maeda*, 2009; *Maeda and Takeo*, 2011], are shown by a solid triangle and open triangles, respectively.

Various models involving magma movement have been proposed to allow a larger variation in the MTCR (e.g., movement between two spheres [*Nishimura et al.*, 2000], among multiple ellipsoidal cavities [*Amoruso and Crescentini*, 2009], and from a sphere to a thin dyke [*Rivalta*, 2010]). We consider magma movement between two ellipsoidal cavities under consideration of total mass conservation, pressure balance and pressure recovery, and we then systematically investigate the effect of cavity geometry on the total MTCR.

3.1. Simple Magma Movement

We consider simple magma movement between two ellipsoidal cavities with arbitrary semiprincipal axes, where mass conservation and pressure balance are preserved. Here "simple" means that it does not include any nonelastic processes causing changes in pressure or volume, such as the generation of gas. We then theoretically derive the resultant moment tensor and examine the possible range of the MTCR.

Magma moves from the high-pressure cavity to the low-pressure cavity to balance the pressure in the system. Hereafter we add a prime to cavity values with the higher initial pressure. We define the initial pressures P_0 and $P_0'(P_0 < P_0')$, the initial volumes V and V', and the initial densities ρ_0 and ρ_0'. We assume the two cavities are filled with the same magma material, and its bulk modulus is denoted by k_m.

The pressure balance after movement is expressed as

$$P_0 + \Delta P = P_0' + \Delta P'. \tag{34}$$

Mass conservation requires

$$\Delta(\rho_0 V) + \Delta(\rho_0' V') = 0. \tag{35}$$

The changes in magma density are

$$\Delta\rho_0 = \rho_0 \frac{\Delta P}{k_m}, \quad \Delta\rho_0' = \rho_0' \frac{\Delta P'}{k_m}. \tag{36}$$

Neglecting the small quantities, equation (35) reduces to

$$V\Delta P\beta = -V'\Delta P'\beta', \tag{37}$$

where β and β' are defined as

$$\beta = \frac{1}{k_m} + \frac{1}{kK^C}, \quad \beta' = \frac{1}{k_m} + \frac{1}{kK^{C'}}. \tag{38}$$

From equations (27) and (37), we obtain

$$\left|\frac{\Delta V^{T'}}{\Delta V^T}\right| = \frac{\beta\Psi K^C}{\beta'\Psi' K^{C'}} = A, \tag{39}$$

where A is defined as the absolute value of the ratio of moment tensor traces (M'_{ii}/M_{ii}) from equation (29). In addition, we use the definition of β to obtain

$$A = \frac{\frac{kK^C}{k_m} + 1}{\frac{kK^{C'}}{k_m} + 1} \frac{\Psi}{\Psi'}. \tag{40}$$

This highlights that A depends on the ratios of the effective bulk modulus of the cavity (kK^C) to the bulk modulus of magma (k_m) and the parameter Ψ. It is noted that A depends on the property of the fluid only through k/k_m, and the coefficient of Ψ/Ψ' in equation (40) monotonically increases or decreases from 1 for $k_m \gg k$ to $K^C/K^{C'}$ for $k_m \ll k$.

Let us assume that the high-pressure cavity is a sphere and $\lambda = \mu$. The values associated with the high-pressure cavity then reduce to

$$\Psi' = \frac{5}{9}, \quad K^{C'} = \frac{4}{5}, \quad M'_{ij}|_{i=j} = k_i \Delta V^{T'}. \tag{41}$$

In addition, we assume $k_m \ll k$, which is valid for magma containing bubbles. Then, equation (40) is reduced to

$$A = \frac{9}{4} K^C \Psi. \tag{42}$$

The assumption is used in the following calculations.

The parameter A has a graphical meaning in the MTCR diagram as follows. The MTCR of the total moment tensor is an external dividing point of the individual MTCR for the high- and low-pressure cavities, and the dividing point is determined by the parameter A as follows:

$$\frac{M_N^{\mathrm{tot}}}{M_{11}^{\mathrm{tot}}} = (1-x)\frac{M_N}{M_{11}} + x\frac{M'_N}{M'_{11}}, \quad x = \frac{\frac{A}{F}}{1+\frac{A}{F}}, \quad (N = 22, 33), \tag{43}$$

and F can then be defined as

$$F = -\frac{1 + \frac{M'_{22}}{M'_{11}} + \frac{M'_{33}}{M'_{11}}}{1 + \frac{M_{22}}{M_{11}} + \frac{M_{33}}{M_{11}}}. \tag{44}$$

F is determined when the MTCR points of the two source cavities are given and $F < -1$ in the present case with a spherical high-pressure cavity. Considering that $A < 1$ due to the geometry dependence of K^C and Ψ, we find $x < 0$.

The blue lines in Figure 3 show the possible range of the MTCR that is covered by the total moment tensor ($M_{ij}^{\mathrm{tot}} = M_{ij} + M'_{ij}$) related to magma movement, with the assumption of a spherical high-pressure cavity. In comparison with Figure 2, this range extends to the lower part of the MTCR diagram ($M_{33}/M_{11} < 1/3$). The lines collapse at a point $\mathrm{X}^{\mathrm{mov}}$, which is the case where the MTCR of the low-pressure cavity is at X.

The red dots in Figure 3a show generalized situations where the high-pressure cavity is not limited to a sphere. The lengths of the semiprincipal axes of the two ellipsoids and their relative orientation are chosen randomly. The calculation procedure is as follows: (i) the diagonalized moment tensors of the two ellipsoids are individually determined in the same way as mentioned above, (ii) one is rotated randomly and added to the other, and (iii) the combined moment tensor is then rediagonalized to obtain the MTCR for the total moment tensor. The density of the red dots can be regarded as the probability of the MTCR for arbitrary sets of ellipsoidal cavities. Figure 3b shows how the total MTCR varies with the relative angles of two cavities for the cases of two crack-like cavities (green dots) and two prolate spheroids (purple dots). The former generates points on PD, while the latter generates a trend along LD, where D and L correspond to a double-couple source and a CLVD source, respectively.

It is important to note that no red dots or blue lines in Figure 3a fall in the area of the MTCR for expanding ellipsoidal cavities (SCP). Therefore, the two mechanisms (expansion and movement) can be clearly distinguished by the MTCR. The two regions merge at P. In the expansion model, P means a penny-shaped crack. In the simple movement model, P means magma movement to a penny-shaped crack from a cavity having K^C larger

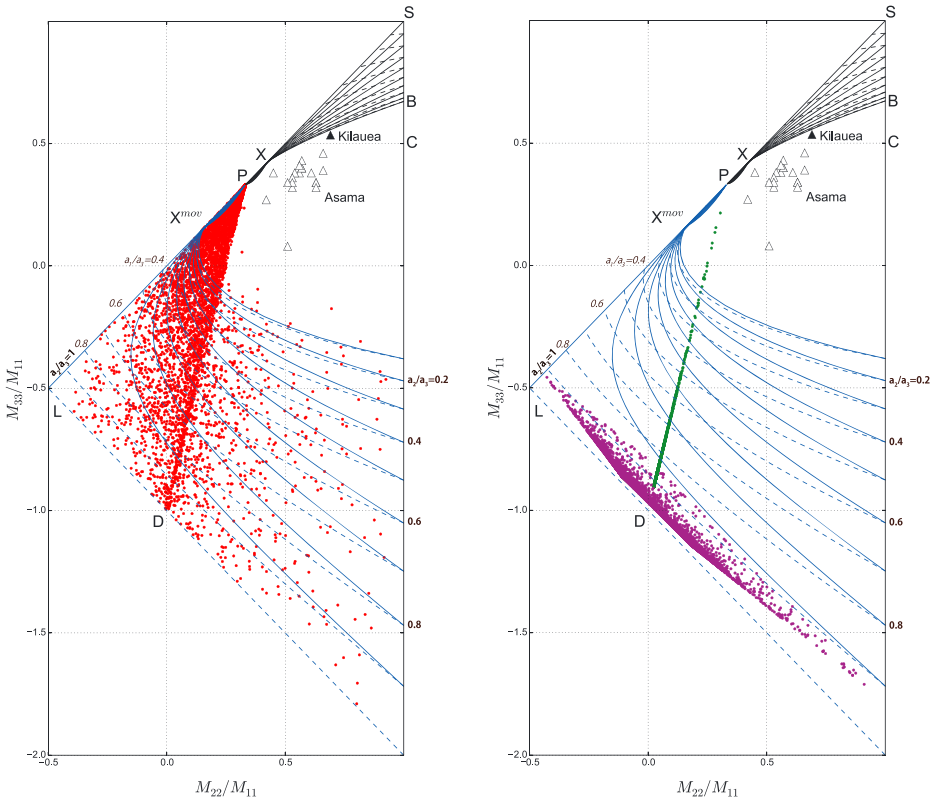

Figure 3. The possible range of total MTCR for simple magma movement. The blue contours are for movements from a spherical high-pressure cavity to an ellipsoid. They are added to Figure 2 with the same definition. D at (0, −1) and L at (−0.5, −0.5) indicate the MTCR values for a double-couple source and a CLVD, respectively. (a) The red dots show the general cases for magma movement between two ellipsoidal cavities. They are produced by calculating the random choices of ellipsoidal geometries and their relative angles. (b) The variation generated by varying relative angles of two penny-shaped cracks and two prolate spheroids are green and purple dots, respectively.

than that of a penny-shaped crack, suggesting that the total moment tensor is dominated by the expansion of the penny-shaped crack.

3.2. Magma Movement With Pressure Recovery

Simple magma movement with increasing degrees of freedom is not yet likely to explain the observations at Asama volcano. The pressure in the cavities after magma movement is higher than the value predicted by the simple model in the presence of pressure recovery processes such as reequilibration [*Nishimura*, 2004; *Ichihara and Nishimura*, 2009]; this section considers magma movement with pressure recovery (Figure 4).

For simplicity, we assume that the expanding cavity is thin (i.e., $a_1 \ll a_3$) and that the high-pressure cavity is a sphere. Then the MTCR of the thin low-pressure cavity moves along the line PB in Figure 3 as a_2 changes between a_1 and a_3. Under these constraints, we estimate the two remaining variables, a_2 and A, for a specific MTCR. We try to explain the representative value of the MTCR observed at Asama volcano [*Maeda and Takeo*, 2011]. The average MTCR is $\left(M_{22}^{\mathrm{obs}}/M_{11}^{\mathrm{obs}}, M_{33}^{\mathrm{obs}}/M_{11}^{\mathrm{obs}}\right) = (0.6, 0.4)$, where the superscript "obs" indicates the observed moment tensor.

First, we calculate a_2 using the relation that the MTCR of the expanding cavity is at the intersection between the line PB and the straight line passing through S and the observed MTCR point. The source geometry is then numerically determined as $a_2/a_3 = 0.70$. Once the MTCR of the cavities and the total MTCR are fixed, we can obtain $A^{\mathrm{obs}} = 0.35$ by using the above mentioned graphical meaning of A.

Due to the dependence of K^C and Ψ on the geometry and the monotonic dependence of A on k/k_m, equation (40) in the simple movement model with $a_1 \ll a_3$ and $a_2/a_3 = 0.70$ suggests $A^{\mathrm{mov}} > 0.80$ for arbitrary k_m, where the superscript "mov" represents the simple magma movement model.

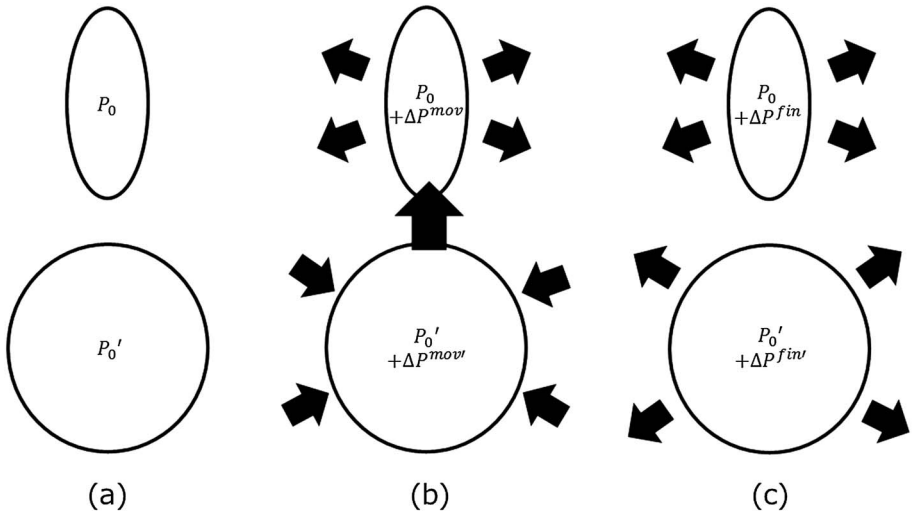

Figure 4. Schematic illustration of magma movement and pressure recovery processes. (a) The initial state. The low-pressure thin ellipsoid with P_0 and the high-pressure sphere with P_0'. (b) After simple magma movement without recovery. Each cavity has a pressure of $P_0 + \Delta P^{\mathrm{mov}}$ and $P_0' + \Delta P^{\mathrm{mov}'}$. (c) The final state. After pressure recovery, the final pressures are $P_0 + \Delta P^{\mathrm{fin}}$ and $P_0' + \Delta P^{\mathrm{fin}'}$, respectively.

We show that the discrepancy between A^{mov} and A^{obs} can be resolved by considering pressure recovery. We define ΔP^{rec} as the pressure recovery, which is equal for the two cavities. Then, the final pressure changes in the individual cavities are

$$\Delta P^{\mathrm{fin}} = \Delta P^{\mathrm{mov}} + \Delta P^{\mathrm{rec}}, \tag{45}$$

$$\Delta P^{\mathrm{fin}'} = \Delta P^{\mathrm{mov}'} + \Delta P^{\mathrm{rec}}, \tag{46}$$

where the superscript "fin" indicates the final values. Dividing equation (46) by $\Delta P^{\mathrm{mov}'}$ and replacing $\Delta P^{\mathrm{fin}'}/\Delta P^{\mathrm{mov}'}$ with $\Delta V^{T\mathrm{fin}'}/\Delta V^{T\mathrm{mov}'}$, according to equation (27), yields

$$\frac{\Delta V^{T\mathrm{fin}'}}{\Delta V^{T\mathrm{mov}'}} = 1 + \frac{\Delta P^{\mathrm{rec}}}{\Delta P^{\mathrm{mov}'}}. \tag{47}$$

Recalling the definition of A and using the relation in equation (27),

$$\frac{A^{\mathrm{obs}}}{A^{\mathrm{mov}}}\frac{\Delta V^{T\mathrm{fin}}}{\Delta V^{T\mathrm{mov}}} = \frac{A^{\mathrm{obs}}}{A^{\mathrm{mov}}}\frac{\Delta P^{\mathrm{fin}}}{\Delta P^{\mathrm{mov}}} = 1 + \frac{\Delta P^{\mathrm{rec}}}{\Delta P^{\mathrm{mov}'}}. \tag{48}$$

Substituting equation (45) into the above equation, we obtain

$$\frac{\Delta P^{\mathrm{rec}}}{\Delta P^{\mathrm{mov}'}} = \frac{A^{\mathrm{obs}}}{A^{\mathrm{mov}}}\left(1 + \frac{\Delta P^{\mathrm{rec}}}{\Delta P^{\mathrm{mov}}}\right) - 1 > \frac{A^{\mathrm{obs}}}{A^{\mathrm{mov}}} - 1. \tag{49}$$

The inequality relation holds because we assume that both ΔP^{mov} and ΔP^{rec} are positive. For Asama volcano, we obtained $A^{\mathrm{mov}} > 0.80$ and $A^{\mathrm{obs}} = 0.35$. It is thus required that more than half of the pressure drop is recovered in the high-pressure cavity after magma movement.

In the above derivation, we assumed that the pressure change due to magma movement and pressure recovery occur at the same time, though the latter process may have a time delay in reality. *Shimomura et al.* [2006] investigated characteristic timescales of the pressure recovery due to reequilibration, demonstrating that the timescale depends mainly on K^C and the volatile diffusivity of magma, and in some conditions it can occur within a short time.

4. Possibilities and Limitations in Constraining Volume Source Processes From Moment Tensors

In volcanology, it is important to interpret the volumetric moment tensor to the mass change of magma and/or gas [*Kazahaya et al.*, 2011, 2015]. To estimate the mass change, both ΔV^C and $V\Delta P$ need to be constrained in addition to the magmatic elastic properties.

The MTCR is insensitive to the geometry near a penny-shaped crack [*Amoruso and Crescentini*, 2009]; the magma movement model exhibits similar uncertainties. The total MTCR for the movement appears where $M_{33}/M_{11} < 1/3$ in Figure 3a, and the uncertainty occurs in the vicinity of PX^{mov}. The dense distribution of the red dots implies that variable sets of geometries and orientations result in similar MTCR values. The results reveal a fundamental difficulty in constraining mass change in cases where the observed MTCR is around PX or PX^{mov}, because of the uncertainties in the source cavity geometry. Mass changes are better constrained when the observed MTCR is far from these values.

As shown in the previous sections, the trace of a moment tensor for the expansion source is $M_{ii} = 3k\Delta V^T$, whereas that of the magma movement model is $M_{ii} = 3k(\Delta V^T + \Delta V^{T'}) = 3k\Delta V^T(1-A)$. For magma movement, the apparent volume change is $\Delta V^T(1-A)$, which is generally nonzero but would be significantly smaller than the real exchange of mass. *Amoruso and Crescentini* [2013] provided a similar statement under the assumption of volume conservation, suggesting that the moving fluid is incompressible. As the parameter A depends on k_m in the form of equation (40), the apparent volume change can be either larger or smaller than their estimates depending on the geometry of the two cavities.

There is another interesting aspect to constraining the source model. We have shown that the total MTCR values resulted from magma movement (Figure 3a). We can see a distinct linear trend along PD in the distribution of the red dots in the figure. The MTCR for magma movement between two penny-shaped cracks falls on D when the cracks are perpendicular to each other and along PD for varying angles (green dots in Figure 3b). On the other hand, *Trasatti et al.* [2011] noted that the MTCR along PD can be expressed by a crack with both tensile and shear dislocations, which is completely different from the magma movement model. Alternatively, this implies that a source apparently dominated by a double couple can be explained by fluid movement rather than a shear dislocation. Further constraints are necessary to distinguish the two mechanisms.

If dense observation in the near field is available, spatial separation of two ellipsoids allows to determine the individual MTCRs with their magnitudes [*Yang et al.* 1992; *Nishimura et al.* 2000; *Maeda and Takeo*, 2011]. In such cases pressure balance and mass conservation, as considered in this work, would give better constraints on the mass of magma involved in the process.

5. Conclusion

A convenient diagram MTCR for a single ellipsoid is extended for two ellipsoidal cavities. We investigated moment tensors associated with the expansion and movement of fluid in ellipsoidal cavities and clarified the possibilities and limitations of source constraints obtained from the observed moment tensors.

It has been shown that the MTCR generated by an expanding ellipsoid is permitted in the area bounded by three geometrical end-members: a sphere, a penny-shaped crack, and a prolate spheroid. The conventional MTCR for a cylindrical source is different from that for a thin spheroid because the strains at both ends of a cylinder have been ignored in the former. The range of the MTCR for an expanding ellipsoid is smaller than that generated by linear combinations of a sphere, a crack, and the conventional cylindrical source. The latter range is still possible when considering two or more expanding ellipsoids.

Next, we examined the MTCR for magma movement between two ellipsoids, where mass conservation and pressure balance are preserved. The MTCR range for magma movement is clearly distinguished from that generated by expanding ellipsoids. The MTCR is calculated by randomly varying the geometry and the relative orientation, and the resultant MTCR is concentrated on the line in the diagram connecting the MTCR for a double-couple source and that for an opening crack. The MTCR in the concentrated range is generated by two thin ellipsoids with various aspect ratios and relative angles. Although such an MTCR is generally interpreted as a crack with both tensile and shear dislocations, it can be generated by fluid movement between two thin ellipsoids.

However, this produces a range of the MTCR that cannot be explained by either fluid expansion or movement. We then considered partial pressure recovery after movement, which likely occurs in volcanic systems. The resultant total moment tensor covered almost all ranges of the MTCR diagram.

There are great uncertainties in the source processes that can be linked to a particular MTCR, which may be determined by observed data. Our method would be useful in interpreting the observed MTCR with a comprehensive view of possible source processes.

Appendix A: Analytical Expression of Ellipsoidal Volume Source

The equation of an ellipsoidal body is

$$\left(\frac{x_1}{a_1}\right)^2+\left(\frac{x_2}{a_2}\right)^2+\left(\frac{x_3}{a_3}\right)^2\le 1, \tag{A1}$$

where a_1, a_2, and a_3 are the three semiprincipal axes. Following *Eshelby* [1957], the symmetry of the tensor S_{ijkl} is

$$S_{ijkl}=S_{jikl}=S_{ijlk}, \tag{A2}$$

and S_{ijkl} is expressed as

$$S_{1111}=Qa_1^2I_{11}+RI_1, \tag{A3}$$

$$S_{1122}=Qa_2^2I_{12}-RI_1, \tag{A4}$$

$$S_{1212}=\frac{Q}{2}\left(a_1^2+a_2^2\right)I_{12}+\frac{R}{2}(I_1+I_2), \tag{A5}$$

where Q and R are

$$Q=\frac{3}{8\pi(1-\nu)}, \tag{A6}$$

$$R=\frac{1-2\nu}{8\pi(1-\nu)}. \tag{A7}$$

I_1, I_{11}, and I_{12} are

$$I_1=2\pi a_1a_2a_3\int_0^\infty\frac{\mathrm{d}s}{(a_1^2+s)\Delta(s)}, \tag{A8}$$

$$I_{11}=2\pi a_1a_2a_3\int_0^\infty\frac{\mathrm{d}s}{(a_1^2+s)^2\Delta(s)}, \tag{A9}$$

$$I_{12}=\frac{2}{3}\pi a_1a_2a_3\int_0^\infty\frac{\mathrm{d}s}{(a_1^2+s)(a_2^2+s)\Delta(s)}, \tag{A10}$$

where

$$\Delta(s)=\left(a_1^2+s\right)^{\frac{1}{2}}\left(a_2^2+s\right)^{\frac{1}{2}}\left(a_3^2+s\right)^{\frac{1}{2}}. \tag{A11}$$

These are known as the Carlson elliptic integrals of the second kind, which can be numerically calculated with arbitrary precision [*Carlson*, 1979; *Press et al.*, 1992]. These equations are employed to calculate D_{ij}, from which Ψ (equation (25)) and K^C (equation (26)) are evaluated.

Acknowledgments
This work was motivated by discussions with R. Kazahaya, Y. Maeda, and H. Kumagai. The final manuscript has been significantly improved by constructive review comments of L. Crescentini. The authors also thank the positive review comments of P. Davis. N.K. was supported by JSPS, KAKENHI25400441. This study was also supported by the Ministry of Education, Culture, Sports, Science and Technology (MEXT) of Japan, under its Earthquake and Volcano Hazards Observation and Research Program. This paper presents a theoretical work and has not used a particular data set. The calculation tools for this study are available from the website http://www.eri.u-tokyo.ac.jp/ichihara/mizuno/index.html.

References

Aki, K., and P. G. Richards (1980), *Quantitative Seismology: Theory and Method*, 1st ed., W. H. Freeman, San Francisco, Calif.
Aki, K., and P. G. Richards (2002), *Quantitative Seismology*, 2nd ed., Univ. Sci. Books, Sausalito, Calif.
Amoruso, A., and L. Crescentini (2009), Shape and volume change of pressurized ellipsoidal cavities from deformation and seismic data, *J. Geophys. Res.*, *114*, B02210, doi:10.1029/2008JB005946.
Amoruso, A., and L. Crescentini (2013), Analytical models of volcanic ellipsoidal expansion sources, *Ann. Geophys.*, *56*(4), S0435.
Carlson, B. (1979), Computing elliptic integrals by duplication, *Numerische Math.*, *33*(1), 1–16.

Chouet, B. A. (1996), New methods and future trends in seismological volcano monitoring, in *Monitoring and Mitigation of Volcano Hazards*, pp. 23–97, Springer, Berlin.

Davis, P. M. (1986), Surface deformation due to inflation of an arbitrarily oriented triaxial ellipsoidal cavity in an elastic half-space, with reference to Kilauea volcano, Hawaii, *J. Geophys. Res.*, *91*(B7), 7429–7438.

Eshelby, J. D. (1957), The determination of the elastic field of an ellipsoidal inclusion, and related problems, *Proc. R. Soc. A*, *241*(1226), 376–396.

Ichihara, M., and T. Nishimura (2009), Pressure impulses generated by bubbles interacting with ambient perturbation, in *Encyclopedia of Complexity and Systems Science*, pp. 6955–6977, Springer, New York.

Kazahaya, R., T. Mori, M. Takeo, T. Ohminato, T. Urabe, and Y. Maeda (2011), Relation between single very-long-period pulses and volcanic gas emissions at Mt. Asama, Japan, *Geophys. Res. Lett.*, *38*, L11307, doi:10.1029/2011GL047555.

Kazahaya, R., Y. Maeda, T. Mori, H. Shinohara, and M. Takeo (2015), Changes to the volcanic outgassing mechanism and very-long-period seismicity from 2007 to 2011 at Mt. Asama, Japan, *Earth Planet. Sci. Lett.*, *418*, 1–10.

Kumagai, H. (2009), Source quantification of volcano seismic signals, in *Encyclopedia of Complexity and Systems Science*, edited by R. A. Meyers, pp. 9899–9932, Springer, Berlin.

Kumagai, H., Y. Maeda, M. Ichihara, N. Kame, and T. Kusakabe (2014), Seismic moment and volume change of a spherical source, *Earth Planets Space*, *66*(1), 7, doi:10.1186/1880-5981-66-7.

Maeda, Y. (2009), Very-Long-Period pulses at Asama Volcano inferred from dense seismic observation, PhD thesis, The Univ. of Tokyo, Japan.

Maeda, Y., and M. Takeo (2011), Very-long-period pulses at Asama volcano, central Japan, inferred from dense seismic observations, *Geophys. J. Int.*, *185*(1), 265–282.

Nishimura, T. (2004), Pressure recovery in magma due to bubble growth, *Geophys. Res. Lett.*, *31*, L12613, doi:10.1029/2004GL019810.

Nishimura, T., H. Nakamichi, S. Tanaka, M. Sato, T. Kobayashi, S. Ueki, H. Hamaguchi, M. Ohtake, and H. Sato (2000), Source process of very long period seismic events associated with the 1998 activity of Iwate volcano, northeastern Japan, *J. Geophys. Res.*, *105*(B8), 19,135–19,147, doi:10.1029/2000JB900155.

Press, W. H., S. A. Teukolsky, W. T. Vetterling, and B. P. Flannery (1992), *Numerical Recipes in C: The Art of Scientific Computing*, Cambridge Univ. Press, New York.

Richards, P. G., and W.-Y. Kim (2005), Equivalent volume sources for explosions at depth: Theory and observations, *Bull. Seismol. Soc. Am.*, *95*(2), 401–407.

Rivalta, E. (2010), Evidence that coupling to magma chambers controls the volume history and velocity of laterally propagating intrusions, *J. Geophys. Res.*, *115*, B07203, doi:10.1029/2009JB006922.

Rivalta, E., and P. Segall (2008), Magma compressibility and the missing source for some dike intrusions, *Geophys. Res. Lett.*, *35*, L04306, doi:10.1029/2007GL032521.

Shimomura, Y., T. Nishimura, and H. Sato (2006), Bubble growth processes in magma surrounded by an elastic medium, *J. Volcanol. Geotherm. Res.*, *155*(3), 307–322.

Trasatti, E., S. Cianetti, C. Giunchi, M. Bonafede, N. P. Agostinetti, F. Casu, and M. Manzo (2009), Bayesian source inference of the 1993–1997 deformation at Mount Etna (Italy) by numerical solutions, *Geophys. J. Int.*, *177*(2), 806–814.

Trasatti, E., M. Bonafede, C. Ferrari, C. Giunchi, and G. Berrino (2011), On deformation sources in volcanic areas: Modeling the Campi Flegrei (Italy) 1982–84 unrest, *Earth Planet. Sci. Lett.*, *306*(3), 175–185.

Wielandt, E. (2003), On the relationship between seismic moment and source volume, Inst. of Geophys., Stuttgart Univ., Germany. [Available at http://www.geophys.uni-stuttgart.de/~erhard/skripte/ew/isomoment/, accessed on May 30 2003.]

Yang, X., P. M. Davis, P. T. Delaney, and A. T. Okamura (1992), Geodetic analysis of dike intrusion and motion of the magma reservoir beneath the summit of kilauea volcano, Hawaii: 1970–1985, *J. Geophys. Res.*, *97*(B3), 3305–3324, doi:10.1029/91JB02842.